

Contents lists available at ScienceDirect

Structures

journal homepage: www.elsevier.com/locate/structures





Influence zones of continuous beam systems

Adrien Gallet ^{a,*}, Andrew Liew ^b, Iman Hajirasouliha ^a, Danny Smyl ^c

- ^a Department of Civil and Structural Engineering, The University of Sheffield, Sir Frederick Mappin Building, Mappin Street, Sheffield, S1 3JD, UK
- ^b Unipart Construction Technologies, Advanced Manufacturing Park, Brunel Way, Rotherham, S60 5WG, UK
- c School of Civil and Environmental Engineering, Georgia Institute of Technology, 790 Atlantic Drive, Atlanta, 30332, GA, USA

ARTICLE INFO

Keywords: Influence zones Influence lines Load arrangements Continuous beams Structural design Pattern loads Polarity zones

ABSTRACT

Unlike influence lines, the concept of influence zones is remarkably absent within the field of structural engineering, despite its existence in the closely related domain of geotechnics. This paper proposes the novel concept of a structural influence zone in relation to continuous beam systems and explores its size numerically with various design constraints applicable to steel framed buildings. The key challenge involves explicitly defining the critical load arrangements, and is tackled by using the novel concepts of polarity sequences and polarity zones. These lead to the identification of flexural and shear load arrangements, with an equation demarcating when the latter arises. After developing algorithms that help identify both types of critical load arrangements, design datasets are generated and the influence zone values are extracted. The results indicate that the influence zone under ultimate state considerations is typically less than 3 adjacent members for any given beam within a continuous system, rising to a maximum size of 5 adjacent members. Additional insights from the influence zone concept, specifically in comparison to influence lines, are highlighted, and the avenues for future research, such as in relation to the newly identified shear load arrangements, are discussed.

1. Introduction

Influence lines, which derive from Betti's theorem established in 1872 [1], are a well-established tool in structural engineering to identify the worst-case load placement on structural systems [2–4], and are widely applied in research related to continuous beam systems [5,6], rigid frames [7], bridge engineering [8] and structural health monitoring [9–11]. Influence zones, on the other hand, also known as zones of influence, are an established concept within the field of geotechnical engineering, helping to identify the area of engineering soils likely to be affected by loading due to sub- and superstructure construction [12], providing geotechnical engineers valuable design insight in deep foundation design [13,14], settlement estimations [15] and preserving groundwater supplies [16].

Despite the obvious discipline link between geotechnical and structural engineering, the equivalent use of an influence zone in structural engineering does not exist in literature. Here, the term *structural influence zone* would refer to the zone in which applied forces, stiffness provisions and support conditions, or changes thereof, impact the design of the surrounding structural system.

The dearth of literature on such an *influence zone* is surprising. For instance, the concept of influence zones also exists outside of geotechnical literature. Some examples are available in research related to the study of saltwater–freshwater interfaces [17], harmful emission

concentrations at traffic intersections [18], reverse k-nearest neighbour algorithms [19,20], propagation path of surfaces waves [21] and ecological studies on below-ground plant competition [22].

Furthermore, one can readily identify situations where knowledge of the influence zone could be beneficial in design. For example, the size of the influence zone could allow an engineer to avoid the need to model an entire structure for the design of a single element whilst being confident that structural information outside the influence zone is irrelevant, with direct applications in multi-disciplinary projects [23]. The impact of late design changes (due to changes in loading or structural provisions), which are known to cause significant time lags until the associated engineering analysis is completed [24], could be more effectively addressed by knowing immediately the selection of members impacted by the said design change. Similarly, engineers are typically required to verify assumptions made in preliminary design [25]. In such cases, the use of an influence zone-based approach could guide what information to incorporate when building an independent model of the design problem. In all of these scenarios, there is valuable design insight to be gained from the influence zone.

This article aims to address the above mentioned knowledge gap by numerically introducing the concept of influence zones in relation to continuous beam systems. First, the theory and procedure for evaluating the influence zone will be introduced in Section 2, followed by the

E-mail address: agallet1@sheffield.ac.uk (A. Gallet).

Corresponding author.

Design of continuous beam systems

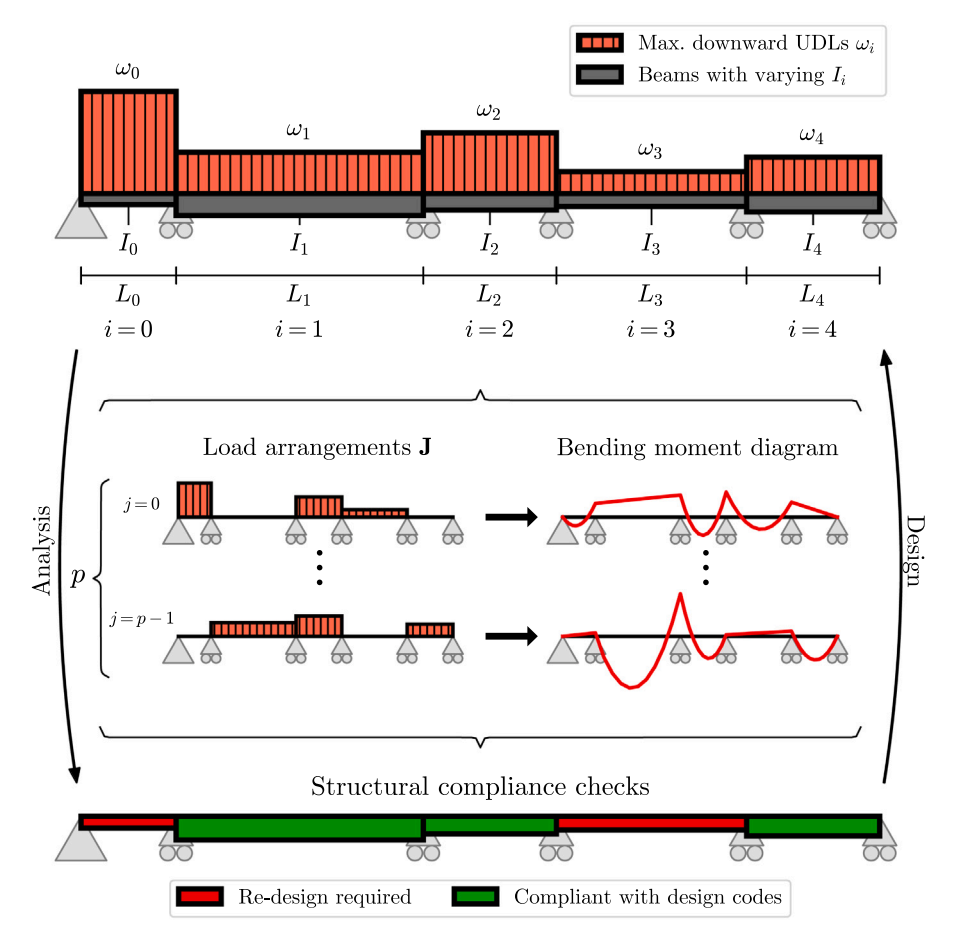


Fig. 1. An exemplary continuous beam system with m = 5 members, subjected to UDLs ω , spans L and with designed cross-sectional properties I, all indexed by i. The system's indeterminacy requires an iterative design process against various load arrangements J of size p indexed by j.

methodology in Section 3 which presents a systematic investigation of critical load arrangements that is key for the evaluation of influence zone values. This allows for the efficient generation of design datasets and the evaluation of their respective influence zones with results presented in Section 4, which are then discussed in Section 5. In addition to the *influence zone*, this paper proposes other novel concepts such as *polarity zones*, identifies an entirely new set of critical pattern loads named *shear load arrangements*, and proposes efficient *load arrangement algorithms* for continuous beam systems of arbitrary member size.

2. Theory

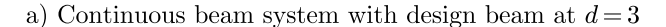
2.1. Overview — continuous beam systems

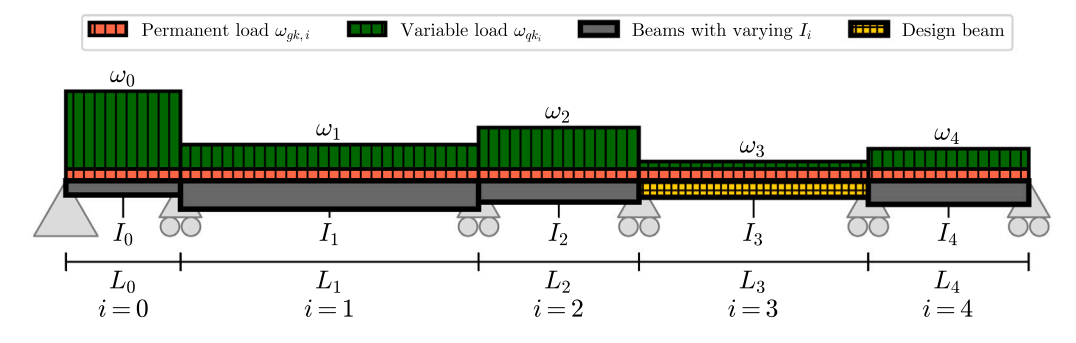
Consider a continuous beam system, as shown in Fig. 1, consisting out of m members, indexed by i, which is subjected to ω_i uniformly distributed loads (UDLs) from vector ω , with each member having span length L_i from vector \mathbf{L} . When designing this system to identify the minimum required structural properties of the members (size optimisation) denoted I_i to form vector \mathbf{I} , it will need to be designed against the worst-case load arrangement (also known as pattern load) from the set of load arrangements \mathbf{J} of size p. The over-restrained nature of this structural system (a function of the support fixity and structural connectivity) renders the continuous beam indeterminate. This means that the performance of the system is a function of the structural properties which need to be evaluated, and generally makes the design

process iterative. Literature has well established formulations to design such indeterminate systems [26].

2.2. Influence zone definition

Suppose a member within a continuous beam system is designated as the design beam by index d as shown in Fig. 2(a), with UDLs ω (which includes both permanent and variable UDL loads $\omega_{g_k,i}$ and $\omega_{q_k,i}$ respectively) and spans L. In the Eurocodes (such as EN1993 [27] for steel systems), the ultimate limit state of a structural member can be expressed by a utilisation ratio u, which ratios over 1.0 denoting structural failure. Using EN1993-1-1 [27], it is possible to determine the true utilisation ratio $u_{d,\mathrm{true}}$ of the design beam d under the critical load arrangement from J if all UDLs ω from the entire system are considered as shown in Fig. 2(b). Now suppose only a sub-selection of all UDLs ω from the adjacently connected spans to that of the design beam d are considered; this sub-selection of UDLs are identified by a discrete integer $k \in \mathbb{Z}$ (where \mathbb{Z} is the mathematical set of all integers) to form vector K. Ignoring all other UDLs, there will be a different critical load arrangement for the design beam d, resulting in a slightly smaller captured utilisation ratio $u_{d,\text{cap}}$ as shown in Fig. 2(c). Whilst $u_{d,\text{cap}}$ will differ from $u_{d,\text{true}}$, the influence zone for member d is defined by $k_{\text{max}} = \max(|\mathbf{K}|)$ (see Fig. 2c) such that the captured utilisation ratio is sufficiently similar to the true utilisation ratio of the design beam; that is $u_{d,\text{cap}} \approx u_{d,\text{true}}$. Note that $k_{\text{max}} \in \mathbb{N}^0$, with \mathbb{N}^0 representing the set of all positive integers and including 0.





b) Critical load arrangement from ${f J}$ that yields $u_{d,\,{
m true}}$

c) Assuming an influence zone $k_{\text{max}} = 2$, ω_0 is ignored, and a different critical load arrangement from **J** yields $u_{d,\text{cap}}$

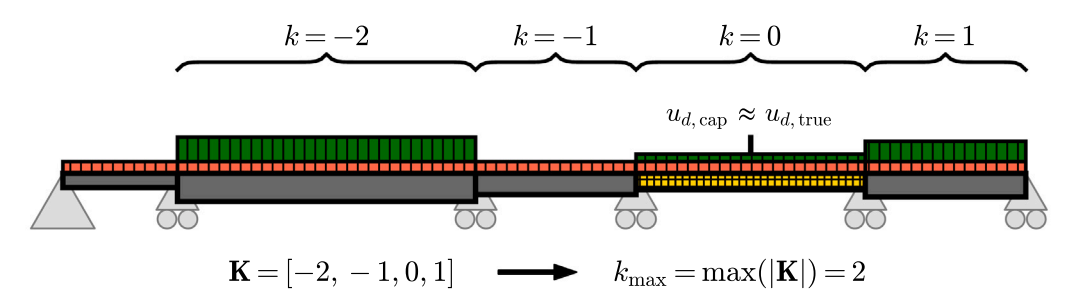


Fig. 2. Key terminology for influence zones: (a) highlights the design beam d, (b) the true utilisation ratio of the design beam $u_{d,\text{true}}$, and (c) the captured utilisation ratio $u_{d,\text{cap}}$ assuming an influence zone of $k_{\text{max}} = 2$.

In this formulation, it is proposed that there should be some value of $k_{\rm max}$ that allows for sufficient approximation of $u_{d,{\rm true}}$. The theoretical foundation for this is based on the realisation that influence lines approach zero when moving away from a given influence line (IL) location as shown in Fig. 3(a). Design information on spans further away from the design beam d therefore have a decreasing influence on the structural response of a design beam d; in other words, there are diminishing returns when considering UDLs ω increasingly distant from a design beam d. For example, using the lengths, UDLs and members of the continuous beam system in Fig. 2(a), the impact in terms of bending moment response of a UDL at an IL location within the design beam *d* can be found by integrating the influence line diagram for each span L_i and multiplying it by the spans UDL ω_i as shown in Fig. 3(b). Using the principle of superposition, the moment contribution about the specified IL location from span i = 0 is therefore small, and would be exceedingly smaller for spans even further from the IL location. The influence zone k_{\max} of a member d is therefore defined as a metric of the design information required to sufficiently approximate the utilisation ratio of that member d.

2.3. Mathematical formulation

A more rigorous formulation is required to identify UDL values ω which cease to be part of a member's influence zone k_{\max} . As explained

previously, the influence zone is established when the captured utilisation ratio sufficiently approximates the true utilisation value, that is $u_{d,\mathrm{cap}} \approx u_{d,\mathrm{true}}$. For a given continuous beam system as depicted in Fig. 1, and the design constraints expressed in Eq. (1),

$$\begin{aligned} & w_{\min} \leq w_i \leq w_{\max} \\ & L_{\min} \leq L_i \leq L_{\max} \\ & I_{\min} \leq I_i \leq I_{\max} \end{aligned} \tag{1}$$

the size of the influence zone of a given design beam d shall be defined when the value of $k_{\max} \in \mathbb{N}^0$: $k_{\max} \in [0,m]$ and all values larger than k_{\max} fulfil the following condition:

$$\left| 1 - \frac{u_{d,\text{cap}}}{u_{d,\text{true}}} \right| \le \epsilon_{\text{max}}$$

$$u_{d,\text{cap}} = \max \left(\sum_{i=-k_{\text{max}}}^{k_{\text{max}}} \mathbf{u}_{d,i,j}(\boldsymbol{\omega}, \mathbf{L}, \mathbf{I}, \mathbf{J}) \right)$$
(2)

where ϵ_{\max} represents the maximum error threshold for the difference between $u_{d,\mathrm{cap}}$, the captured utilisation ratio of the design beam d for a given value of k_{\max} , and $u_{d,\mathrm{true}}$, the true utilisation ratio of the design beam d if the contribution of all UDLs of the continuous beam system had been considered. Note that, not shown in Eq. (3) is that the value of i cannot exceed the maximum number of adjacently lying spans within the system. $\mathbf{u}_{d,i,j}$ is the utilisation ratio contribution function towards the design beam d by member i based on the UDLs

a) Bending moment $M_{u,IL}$ influence line (IL) about specified location

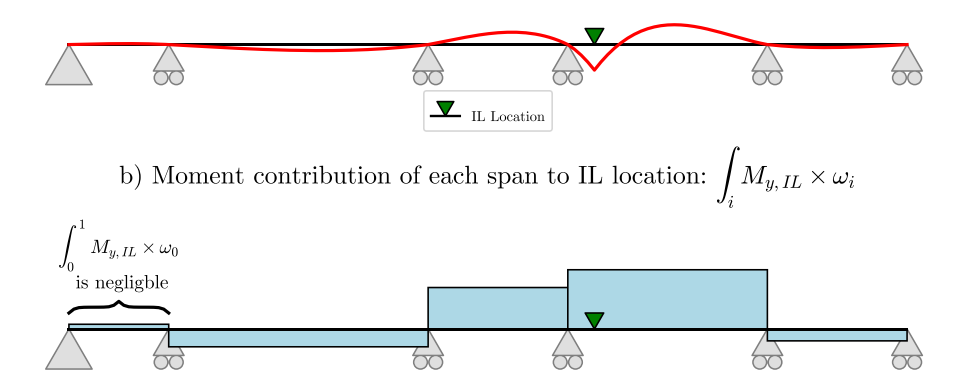


Fig. 3. The influence of UDLs to the bending moment experienced at an influence line (IL) location becomes increasingly negligible the further away one moves from the IL location.

 ω , spans L, structural properties I and load arrangements J indexed by j. For the particular case of a continuous beam system loaded by UDLs as presented in Fig. 1 it is possible to define the utilisation ratio contribution function $\mathbf{u}_{d.i.i}$ as:

$$\mathbf{u}_{d,i,j} \to \mathbf{D}_{\mathrm{ULS}}(I_d, M_{d,i,j}, V_{d,i,j})$$

$$M_{d,i,j} = \omega_i \ J_{i,j} \int_i \mathbf{M}_{\mathrm{IL},d}$$

$$V_{d,i,j} = \omega_i \ J_{i,j} \int_i \mathbf{V}_{\mathrm{IL},d}$$
(3)

where $\mathbf{D}_{\mathrm{ULS}}$ represents the ULS steel cross-section design checks based on the appropriate Eurocodes of the material considered (such as EN 1993-1-1 6.2 [27]), I_d represents the cross-sectional properties, $M_{d,i,j}$ denotes the major axis moment while $V_{d,i,j}$ is the major axis shear force of the design beam d, w_i is the UDL, and $J_{i,j}$ is the activation factor (a value 0 or 1) from one possible critical load arrangement J_j of all viable critical load arrangements $\mathbf{J}_{\mathrm{crit}}$. Integrals $\int_i \mathbf{M}_{\mathrm{IL},\mathrm{d}}$ and $\int_i \mathbf{V}_{\mathrm{IL},\mathrm{d}}$ are the integrated influence line values across beam i for a particular influence line location within the design beam d as introduced in Fig. 3(b).

The mathematical formulation as written in Eqs. (2) and (3) determines the value of $k_{\rm max}$ at which the contributions outside of the influence zone become exceedingly small by measuring the difference between $u_{d,{\rm cap}}$ and $u_{d,true}$ relative to $\epsilon_{\rm max}$. As $k_{\rm max}$ increases, the ratio $u_{d,{\rm cap}}/u_{d,{\rm true}}$ will approach unity, attaining unity if all structural members of the system are considered within the influence zone since the influence of all members is in that case accounted for. If the error threshold $\epsilon_{\rm max}$ is relaxed, an influence zone less than the total size of the system can be found.

2.4. Visualised influence zone evaluation procedure

The evaluation procedure used to find the influence zone value $k_{\rm max}$ based on a predefined $\epsilon_{\rm max}$ using Eqs. (2) and (3) is visualised in Fig. 4. This particular example deals with a m=15 homogeneous system (identical spans L and UDL ω for all members) consisting out of hotrolled S355 steel UB178 \times 102 \times 19 cross-sections [28] each spanning 4 m. It is assumed that an un-factored permanent (dead) $\omega_{g_k,i}=3\,{\rm kN/m}$ and a variable (live) $\omega_{q_k,i}=15\,{\rm kN/m}$ load act on each span as shown in Fig. 4(a).

A detailed explanation of the influence zone evaluation procedure as presented in Fig. 4a follows next. Suppose one intends to establish the influence zone value for design beam d=4 with an $\epsilon_{\rm max}=0.01$. In other words, how many adjacent UDL loads to those of the design member at index i=4 need to be considered to capture 99% of the true utilisation ratio $u_{d,\rm true}$. As the first step, one assumes an influence zone of $k_{\rm max}=0$

as shown in Fig. 4(b); this ignores all UDL values except for those on the design beam d. Using Eurocode load factors and combinations [29], the captured utilisation for an influence zone $k_{\rm max}=0$ is $u_{d,{\rm cap}}=0.5101$. In the next step, shown in Fig. 4(c), the influence zone is increased to $k_{\rm max}=1$. Note that the critical load arrangement now occurs when members i=3 and i=4 experience the full variable (live) load. The captured utilisation ratio in this instance is $u_{d,{\rm cap}}=0.7191$. The influence zone value is then increased again to $k_{\rm max}=2$ as shown in Fig. 4(d). Notice that the critical load arrangement now occurs when spans i=2,4,5 are fully loaded, and yields a captured utilisation ratio of $u_{d,{\rm cap}}=0.7293$. By continuously increasing the assumed value of $k_{\rm max}$ and identifying the critical load arrangement for that particular assumed influence zone value, one yields the captured utilisation ratio $u_{d,{\rm cap}}$. This is precisely what is expressed by Eqs. (2) and (3).

The assumed influence zone value can be continuously increased to $k_{\rm max}=3,4$, etc., and their associated captured utilisation ratio $u_{d,{\rm cap}}$ evaluated as shown in Fig. 4(e) and (f). Eventually, the influence zone captures the entirety of continuous system, as shown by $k_{\rm max}=10$ in 4(g). In this instance, the utilisation ratio represents the true utilisation ratio $u_{d,{\rm true}}$ of the design system, since it considers all UDL loads. In this instance, $u_{d,{\rm true}}=0.7560$.

Knowing the true utilisation ratio, it is now possible to evaluate which influence zone value $k_{\rm max}$ fulfilled the conditions identified by Eq. (2). In this example, an influence zone value of $k_{\rm max}=3$ corresponded with a captured utilisation ratio $u_{d,{\rm cap}}=0.7536$; since $\left|1-\frac{u_{d,{\rm cap}}}{u_{d,{\rm true}}}\right|=\left|1-\frac{0.7536}{0.7560}\right|=0.0032 \le \epsilon_{\rm max}=0.01$, and because it can be shown this holds true for all larger values of $k_{\rm max}$, the influence zone value for design beam d=4 with an error of less than $\epsilon_{\rm max}=0.01$ is $k_{\rm max}=3$.

The example above demonstrates the procedure to evaluate the influence zone value for one member within a particular continuous beam system containing a specific set of UDL ω and span L values. By itself, this type of evaluation would already provide some utility to structural designers to understand, for example, if a new UDL load will significantly impact a beam design depending on whether it falls within that beam's influence zone.

However, the influence zone value is ultimately also a function of the *range* of UDLs, spans and cross-section properties that can arise. Consider for example that the influence zone of a continuous beam systems with UDLs of infinite magnitudes will always be the entire system size, regardless of the $\epsilon_{\rm max}$ value. For these reasons, it is of interest to study the statistical distribution of influence zone values for beam systems under pre-defined design constraints as defined by Eq. (1). By systematically generating a multitude of different continuous beam

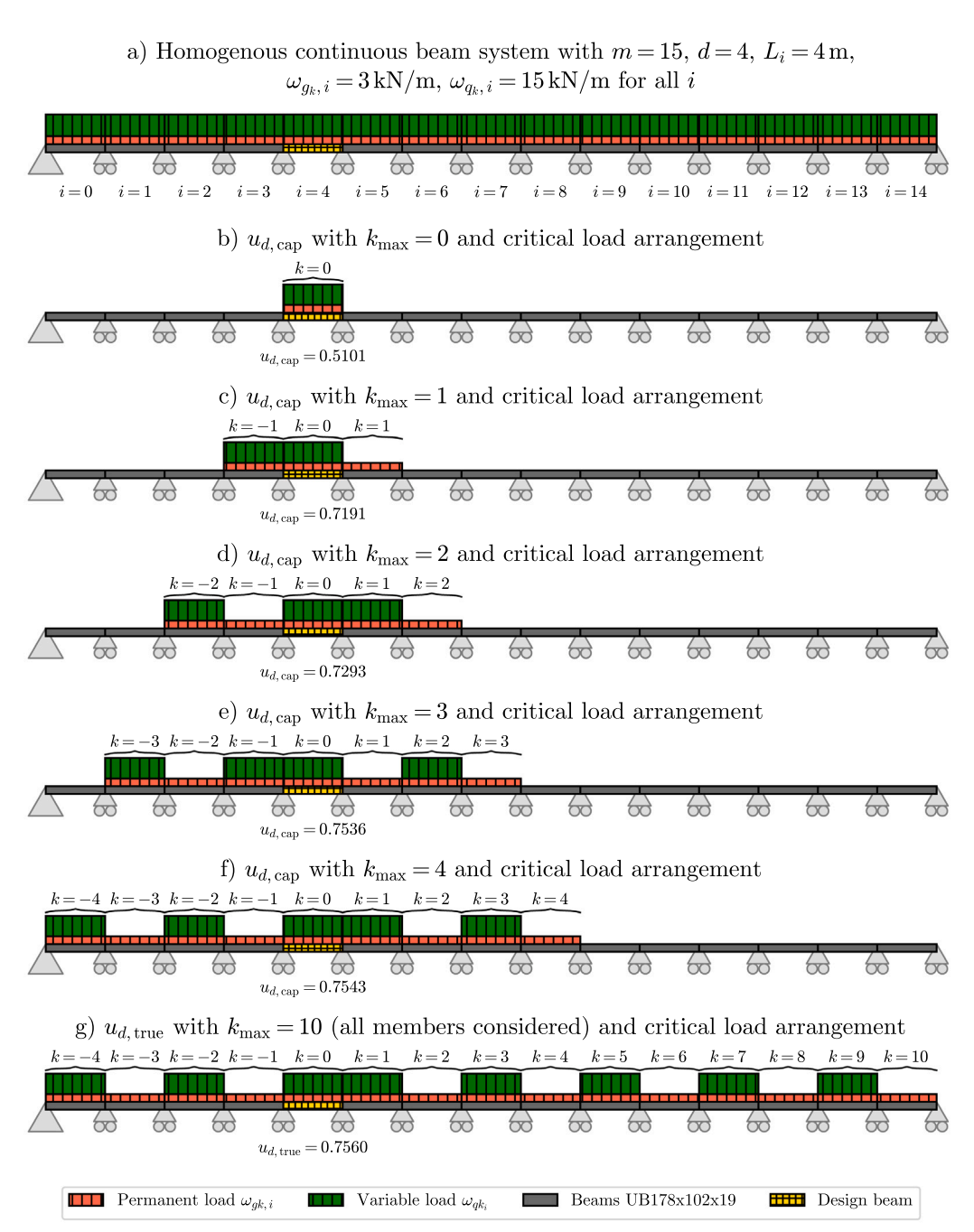


Fig. 4. A visualised example of the influence zone evaluation procedure. The procedure begins with an existing beam system loaded as shown in (a), and then evaluates the captured utilisation $u_{d,\text{cap}}$ for various values of k_{max} in (b)–(f). The appropriate influence zone value becomes a function of ϵ_{max} that ensures the captured utilisation ratio is sufficiently close to the true utilisation ratio evaluated in (g).

systems, identifying the critical load arrangements, and evaluating the influence zone of each member within those systems, influence zone values can be studied in their aggregate. This can lead to prior knowledge of the size of the influence zone for members within a continuous beam system, which in turn could be of interest to practising structural engineers as explained in Section 1.

2.5. The key challenge

Most of the information required in Eqs. (2) and (3) can be easily found. Influence lines are relatively easy to extract for a continuous beam system, and integrating these for Eq. (3) is numerically simple. The cross-section design checks $\mathbf{D}_{d,i,j}$ are clearly defined by design

codes, and the summation for of the individual utilisation ratio contributions in (2) is trivial. However, from the visualised example shown in Fig. 4, it should be evident that accurate knowledge of the critical load arrangement for the entire system as well as for different sizes of the assumed influence zone value is required.

To find the critical load arrangements for Eqs. (2) and (3), one could use a naive, brute-force procedure to trial every possible load arrangement to create the set J_{naive} with a corresponding set size of $p_{naive} = 2^m$. This is not an issue for systems with few members, but if larger systems, such as the m = 15 system shown in Fig. 4, need to be modelled to study the influence zone in depth, a brute-force approach becomes computationally expensive. For example, the m = 15 system has $p_{naive} = 2^m = 32,768$ possible load arrangements, and only a smaller set of these can actually ever be critical. The issue of computational

Table 1 Design constraints for various design scenarios used in this investigation based on Eurocode terminology, with G_k and Q_k being the characteristic permanent and variable actions. Increasing set numbers correspond to increasing design variation, a proxy for design complexity. Span and UDL values are discretised in 0.5 m and 5 kN/m increments respectively.

Dataset	$\omega_{g_k,i} =$	$\omega_{q_k,i} \in$	$L_i \in$		
Set 1 — Zero variation	3.0 kN/m	a for all i , with $a \in [0 \text{ kN/m}, 60 \text{ kN/m}]$	b for all i, with $b \in [1 \text{ m}, 12 \text{ m}]$		
Set 2 — Low variation	3.0 kN/m	$[20\mathrm{kN/m},40\mathrm{kN/m}]$	$[4\mathrm{m}, 8\mathrm{m}]$		
Set 3 — Medium variation	3.0 kN/m	$[10\mathrm{kN/m},50\mathrm{kN/m}]$	[2 m, 10 m]		
Set 4 — High variation	3.0 kN/m	$[0\mathrm{kN/m},60\mathrm{kN/m}]$	[1 m, 12 m]		

cost in relation to critical load arrangements of large-scale systems is well acknowledged in literature, and various methodologies have been employed using probability [30] and possibility theories [31,32]. Among the latter, fuzzy sets using interval finite-element methods have been shown to be efficient and accurate [33,34].

However, whilst these interval-based methods are effective at evaluating the bounds (the worst case force/moment value) due to the critical load arrangement, they do not in fact reveal what this load arrangement looks like. This is problematic for the evaluation of the influence zone, since Eq. (3) relies on being able to identify this set J explicitly in terms of the individual activation factors $J_{i,j}$ (either 0 or 1) that make up the load arrangement J_j . Another approach would be to use the load arrangements prescribed by design manuals, yet these consist out of a heuristic set of load arrangements that are known to be non-conservative [34].

Due to these limitations, the methodology in Section 3 focuses on developing a systematic and universal procedure to evaluate the critical load arrangements $J_{\rm crit}$ of any continuous beam system of size m. The procedure will also focus on being applicable to both homogeneous (identical spans, UDLs and beam properties for all members) and heterogeneous systems. This knowledge will also feed directly to generating design datasets of continuous beam systems efficiently under various design constraints. Section 4 presents the results, first validating the critical load arrangement procedure established in this work, and subsequently finding the influence zone values for continuous beam systems under various design constraints.

3. Methodology

3.1. Assumptions and design constraints

This investigation will make the following design and modelling assumptions. First, cross-sectional properties are restricted to prismatic BS EN 10365:2017 UKB I-sections [28] made out of S355 steel with perfectly linear elastic behaviour using Timoshenko–Ehrenfest beam theory (yet the design was conducted using plastic section properties as allowed by EN 1993-1-1 5.4.2(2) [27]). It was assumed that all spans are laterally restrained (and hence not susceptible to lateral instability), with elements designed against EC3 ULS checks (and notably not SLS requirements) with EN 1990 Eq. 6.10 load combination factors [29]. These design assumptions were used in all modelling software.

The design constraints considered for Eq. (1) were chosen for their relevance in the design of continuous steel framed buildings, and is reflected by the range of UDLs and spans of the design datasets. Four individual design scenarios are considered to study the influence zone in depth, with each set featuring an increasing variation in span lengths and applied loads, summarised in Table 1. Length and UDL values are discretised in 0.5 m and 5 kN/m increments respectively, and are drawn from a random uniform distribution, thereby providing an increasingly higher level of heterogeneity in Sets 2, 3 and 4.

3.2. Critical load arrangements

The critical load arrangement identification procedure relies on two new concepts, namely *polarity sequences* and *polarity zones*. Both of these concepts form the basis to systematically identify the critical load arrangement set $J_{\rm crit}$.

3.2.1. Polarity sequences

Influence lines can be used to identify the critical load arrangements for a given continuous beam system. By integrating the influence line of each member *i*, one can evaluate the net contribution (positive or negative) a UDL causes in terms of bending moments and shear forces at the influence line (IL) location. The net-contribution of each beam can be either positive or negative at the IL location, that is "hogging or sagging" for bending moments and "clockwise or anti-clockwise" for shear forces, respectively, which is termed as the *polarity* of that particular beam. This procedure is shown in Fig. 5(a) to (b).

Since the design problem is restricted to positive UDL values only (see Table 1), it is possible to construct a *polarity sequence* for a particular IL location, as shown in Fig. 5(c). When all beams of positive polarity are loaded, then the maximum positive internal forces are generated at the IL location, and vice-versa, loading the negative polarity members leads to the maximum negative internal forces.

3.2.2. Polarity zones

A rigorous qualitative study of the polarity sequences for different IL locations and design scenarios revealed 5 unique polarity sequences that occur along specific segments of a given beam span termed *polarity zones*, which are illustrated in Fig. 6 for the central beam highlighted in red.

These 5 polarity zones are common to all members of both homogeneous (equal spans and cross-sections) as well as heterogeneous continuous beam systems, although the exact boundaries between one zone varied depending on the relative magnitude of spans and cross-section properties. The sequences identified in Fig. 6 also extend to larger beam systems with the polarity direction alternating at each successive beam. For example, if the 5-member system was extended by an additional member on either side of the system (to give a 7 member system), the left-most member of the Type I polarity sequence would have a positive polarity, and similarly, the right-most member would have a negative polarity. The same logic extends to the other four sequences.

Each polarity sequence is indicative of two critical load arrangements that maximise the positive or negative internal member forces respectively. The maximum positive load arrangement for Type I is also equal to the maximum negative load arrangement for Type IV, since these sequences are polar opposites of each other, which is also true for the Type II and Type V sequences. Consequently, these 5 polarity zones correspond to 6 unique critical load arrangements for a given beam, namely positive Type I, II and III along with their (negative) polar opposites. The only exceptions occur for the beams at either end of the spans, named end-span beams, in which the Type I and Type IV sequences collapse into the Type III sequence (or its polar opposite) at the left end, and similarly for the Type II and Type V sequences at the right end, resulting in four unique load arrangements for end-span beams.

3.2.3. Flexural load arrangements

It is now possible to identify the first set of critical load arrangements for continuous beam system, defined as the flexural load arrangements $\mathbf{J}_{\mathrm{flex}}$. Although each non-end-span beam has 6 unique critical load arrangements, it does not mean that a continuous beam system has 6m unique load arrangements (m is the number of members in the beam system). This is because, as shown in Fig. 7, the maximum positive Type V load arrangement for one beam is identical to the maximum positive Type I load arrangement of the beam immediately adjacent to (the right

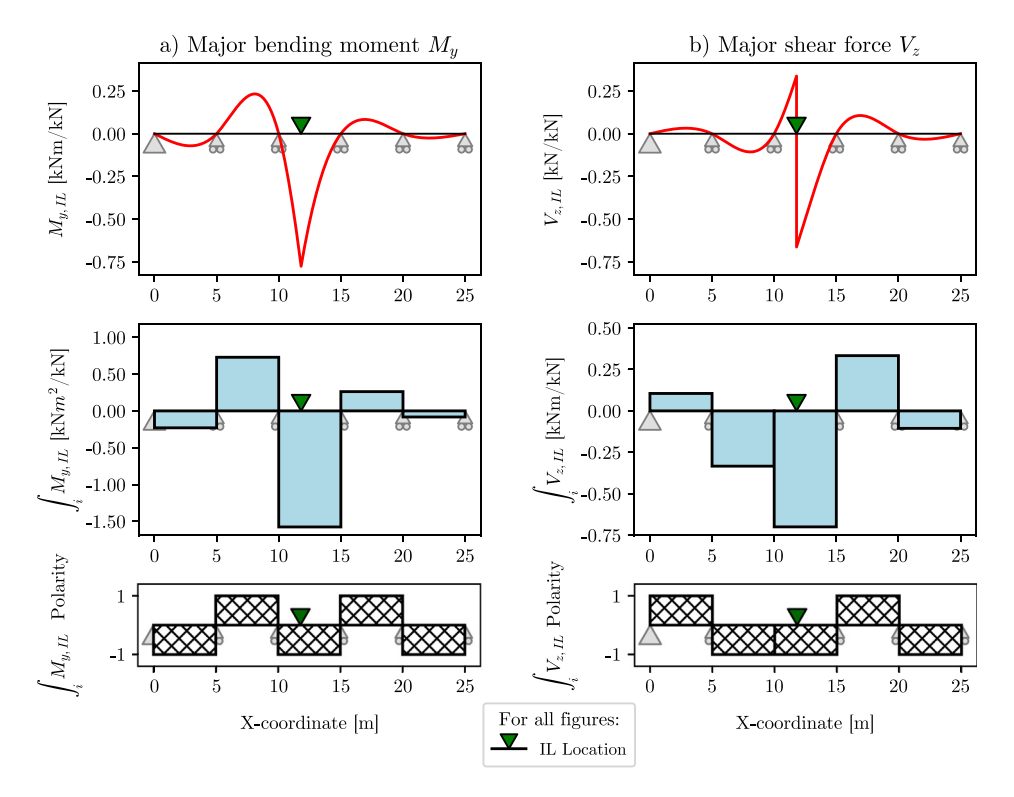


Fig. 5. An exemplary process of arriving from influence line plots (top row) to polarity sequences (bottom row) via integrated influence lines (middle row) for (a) major axis bending moment M_v and (b) major axis shear force V_v about the specified influence line (IL) location.

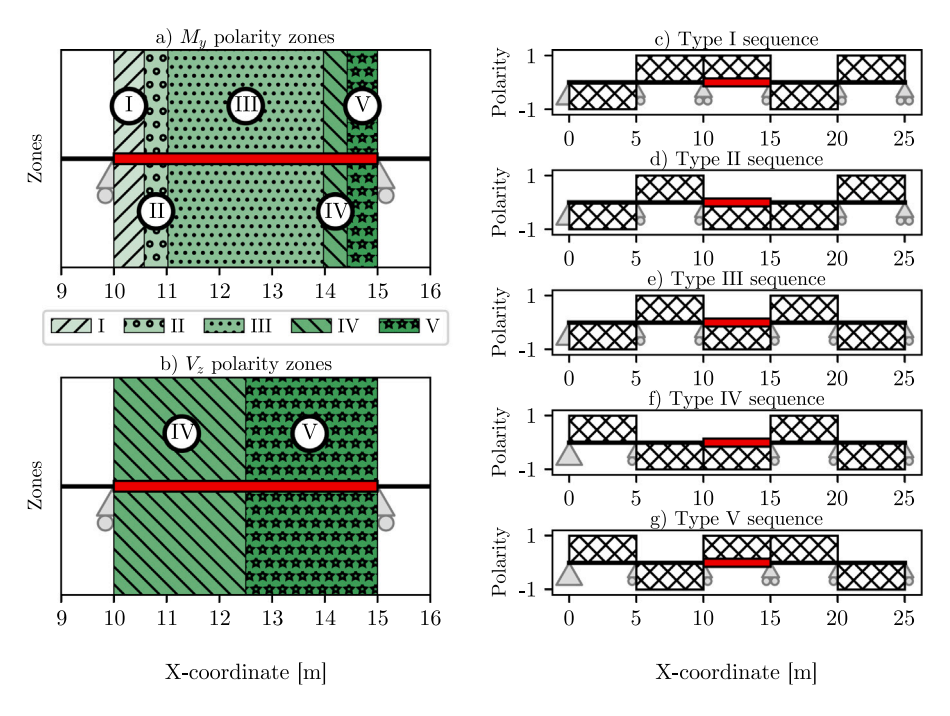


Fig. 6. Polarity zones that occur along various span segments of a m = 5 homogeneous beam system of equal span and cross-sectional properties. The same zones and sequences, although at different boundaries, occur in heterogeneous (varying UDL and span) systems. (For interpretation of the references to colour in this figure legend, the reader is referred to the web version of this article.)

of) it. A similar overlap exists between Type II and Type IV sequences, and the two Type III load arrangements (for maximum and negative internal forces) are identical for all beams.

Through a process of elimination, it is possible to simplify the actual total number of potential critical load arrangements to $p_{\rm flex}=2m$. Algorithm 1 provided in Appendix A can be used to evaluated ${\bf J}_{\rm flex}$. An example output for a m=5 system is shown in Fig. 8, highlighting

the $p_{\mathrm{flex}}=2m=10$ critical load arrangements J_j , along with their individual activation factors $J_{i,j}$. The load arrangement set $\mathbf{J}_{\mathrm{flex}}$ of size $p_{\mathrm{flex}}=2m$ identified here represents a literal exponential improvement in terms of computational cost when compared to the brute-force approach of analysing and designing against $p=2^m$ load arrangements and for evaluating the influence zone with Eq. (2).

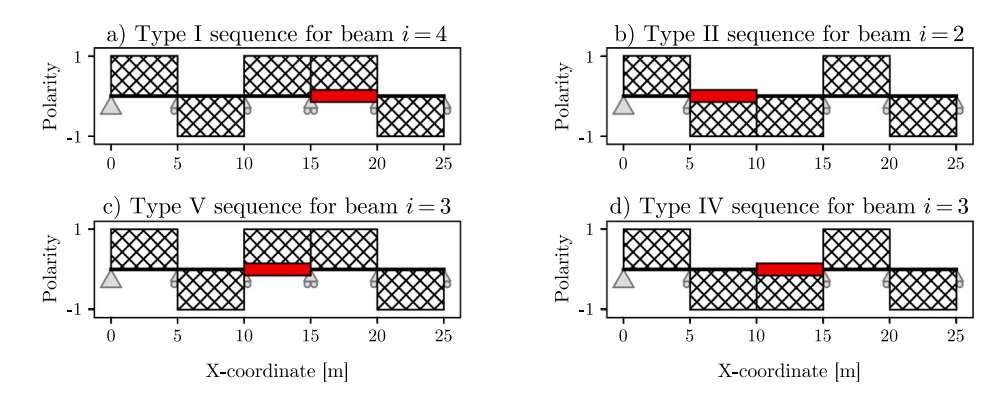


Fig. 7. Polarity sequences are identical for adjacently lying beams (highlighted in red) for Type I and Type V sequences as shown by Figure (a) and Figure (c), as well as Type II and Type IV sequences, as shown by Figure (b) and Figure (d). (For interpretation of the references to colour in this figure legend, the reader is referred to the web version of this article.)

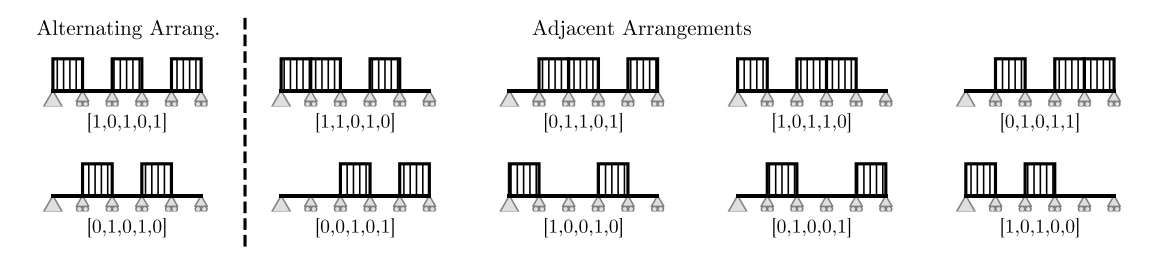


Fig. 8. The critical load arrangements set J_{flex} of size p = 2m for a 5-member continuous beam system (p = 10) grouped in alternating and adjacently loaded arrangements. Each load arrangement J_i consists out of $J_{i,i}$ activation factors of value 0 or 1.

3.2.4. Shear load arrangements

During initial validation of whether $\mathbf{J}_{\mathrm{flex}}$ contained all the critical load arrangements $\mathbf{J}_{\mathrm{crit}}$ (i.e. $\mathbf{J}_{\mathrm{crit}} \in \mathbf{J}_{\mathrm{flex}}$), other unique critical load arrangements were identified. Analysing these special cases in detail indicated that these different critical load arrangements occurred when the span of a member L_i was less than a certain L_{shear} span limit quantified by:

$$L_i < \sqrt{\frac{6EI_{yy,i}}{GA_{z,i}}} \approx L_{\text{shear}}$$
 (4)

where E and G are the Young's and shear modulus of the material respectively, L_i is the span of the beam, and $I_{yy,i}$ and $A_{z,i}$ were the major second moment of area and shear area of the prismatic beam, respectively.

Although the $L_{\rm shear}$ span limit appears to be related to shear beams, this is the first time that shear beams have been reported in literature to cause novel critical load arrangements. The shear limit identified by Eq. (4) was derived by studying the differences between the more commonly used Euler–Bernoulli beam theory with the Timoshenko–Ehrenfest theory [35], specifically as expressed in their stiffness matrix form. As shown in Fig. 9, shear beams appear to flip the polarity of the immediately adjacent member when measured outwardly from a given IL location, with all subsequent members alternating the polarity direction as before.

When shear beams (as defined by the $L_{\rm shear}$ limit) occur, new critical load arrangements arise that are currently not contained within ${\bf J}_{\rm flex}$. The increase in terms of the final utilisation factor of the beams was typically in the range of 4%–5%, although larger increases were also observed. Whilst a thorough analysis of the increase in utilisation ratio caused by these newly identified load arrangements would be of interest, it falls outside the scope of this study. The validity of Eq. (4) for all design conditions, especially for different cross-sections, as well as the physical cause for the unique influence line patterns shown in Fig. 9(b) would require further investigations.

Instead, an algorithm will be presented capable of identifying these new load arrangements, which is necessary for the evaluation of the influence zone. The principal issue when evaluating the shear beam induced critical load arrangements, hereafter referred to as the *shear load arrangements* $\mathbf{J}_{\text{shear}}$, is the fact that the final material and cross-sectional properties to evaluate the L_{shear} limit in Eq. (4) are not known until the beam is designed. This creates a causality dilemma which needs to be addressed.

In clear opposition to the $J_{\rm flex}$ set, which does not depend on the continuous beam system properties, the shear load arrangements cannot be established *in universum* without some system knowledge. However, by taking advantage of the design constraints set by Eq. (1), which are defined in Table 1, one can identify *a priori* what members are susceptible to cause shear load arrangements by re-writing Eq. (4) as:

$$\sqrt{6\left(\frac{E}{G}\right)_{\text{max}}\left(\frac{I_{yy}}{A_z}\right)_{\text{max}}} < L_{\text{shear,max}}$$
 (5)

The above equation groups the maximum material and cross-sectional property ratios together. By limited the design space to S355 steel and UB section sizes as specified in Section 3.1, the maximum material ratio ($(E/G)_{\rm max}=2.600$ using EN 1993-1-1 material properties [27]) and cross-sectional property ratio ($(I_{yy}/A_z)_{\rm max}=0.397$ m²) can be evaluated (based on BS EN 10365 [28] cross-sections). Beams shorter than the shear span limit are susceptible to cause shear load arrangements (in this case $L_{\rm shear,max}=2.49$ m). In identifying these susceptible members, it is possible to evaluate the shear load arrangements using Algorithm 2 provided in Appendix B.

Algorithm 2 transforms the flexural load arrangement from set $\mathbf{J}_{\mathrm{flex}}$ based on a list of susceptible shear beams identified by Eq. (5). This is achieved by flipping the on/off activation factor (the 0 or 1 in $J_{i,j}$) of the load arrangement if a shear beam is encountered whilst travelling outwardly in both the left and right direction from a start beam index. This operation transforms the flexural load arrangement based on the behaviour identified visually in Fig. 9, and needs to check four individual case conditions to account for continuous beam systems that have multiple, potentially adjacently lying, shear beams.

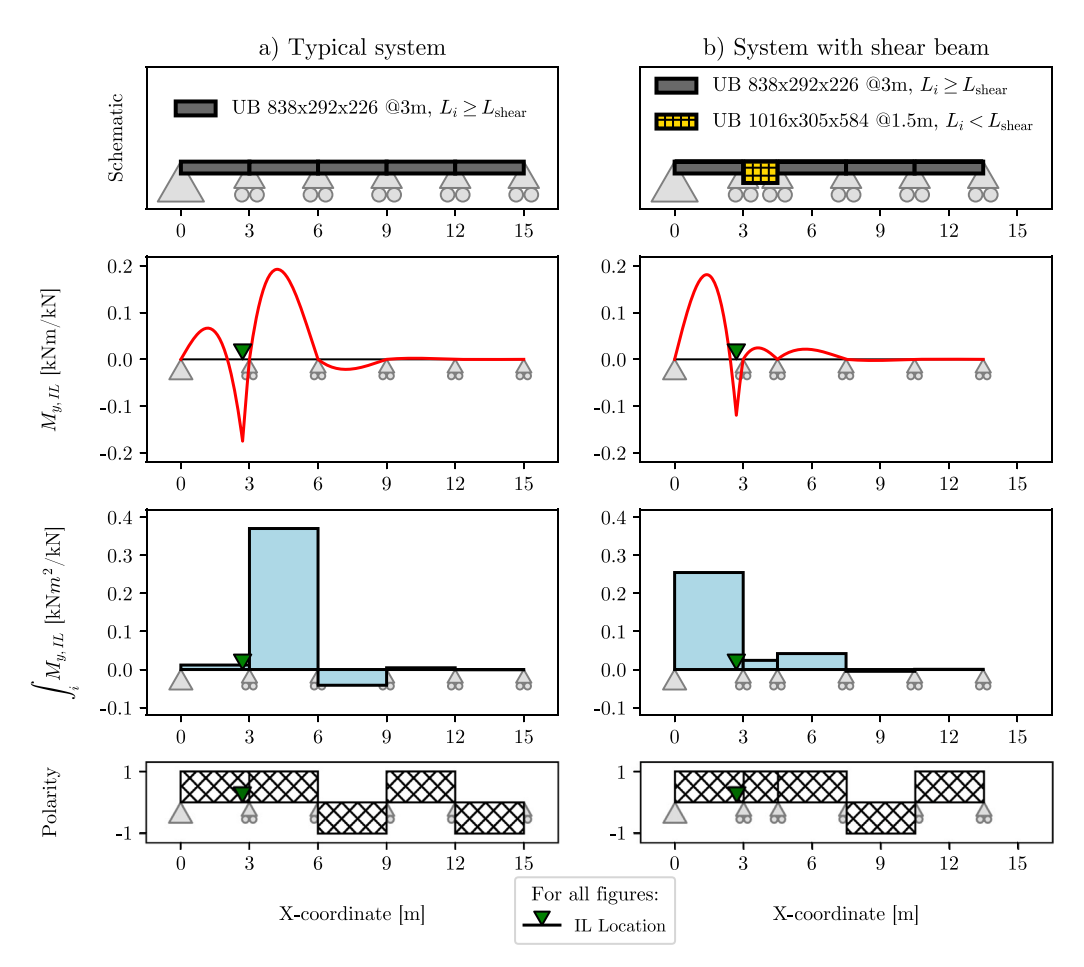


Fig. 9. A schematic demonstrating the impact of a shear beam (highlighted in yellow) on a standard polarity sequence of a continuous beam system when spans shorter than the shear span limit L_{shear} (as identified by Eq. (4)) occur. A deeper beam is used on the second span to increase the effects of this influence line pattern. Note the flipped polarity directions of the members on the right-hand side of the system. (For interpretation of the references to colour in this figure legend, the reader is referred to the web version of this article.)

Since every beam system is of size m, the time complexity of a single pass of Algorithm 2 is O(m). However, since every flexural load arrangement (2m), and every combination of n potential shear beams (2^n-1) combinations, as the zero set is already considered in \mathbf{J}_{flex} by default), and every possible start-index (m) needs to be computed, the time complexity to evaluate the shear set $\mathbf{J}_{\text{shear}}$ would be $O(m^3 2^n)$. It should be noted that this process is computationally expensive.

It was observed that passing every possible start index generated either duplicate shear load arrangements, or occasionally existing flexural load arrangements. For example, for a given singular potential shear beam location, the algorithm would result in the same transformed shear load arrangement for all start-indices starting on the left and right hand-side of that susceptible shear beam location. Similarly, the two alternating arrangements from \mathbf{J}_{flex} would result in an already existing adjacent arrangement from \mathbf{J}_{flex} if only a singular susceptible shear beam exists.

Using such logic, it is sufficient to pass only adjacent arrangements from \mathbf{J}_{flex} along with the left-hand (or right-hand) index of the adjacently loaded spans as the start index for Algorithm 2 to yield an effective set of potential shear load arrangements. By not having to evaluate Algorithm 2 for every possible start index of each load arrangement, the computational complexity reduces to $O(m^2 \, 2^n)$. From this, it also follows that since the alternating load arrangement is never transformed (which leaves only 2(m-1) load arrangements to be passed to the algorithm) and since 2^n-1 possible shear beam combinations can exist, the maximum number of unique critical shear load arrangements should be of size $p_{\text{shear}} = 2(m-1)(2^n-1)$.

3.2.5. Validation test of critical load arrangements for continuous beams

By adding the set of flexural and shear load arrangements together, it should be possible to explicitly define the set of critical load arrangements for any continuous beam system under defined design constraints. A validation test was conducted to check if $J \rightarrow J_{\text{crit}} \in$ $\mathbf{J}_{\text{flex}} \cup \mathbf{J}_{\text{shear}}$, with the results presented in Section 4. The validation test was achieved by generating 1024 heterogeneous continuous beam systems with m = 10 members with spans $L_i \in [1 \,\mathrm{m}, 12 \,\mathrm{m}]$, permanent (dead) UDL $\omega_{q_k}=3$ kN/m and variable (live) UDLs $\omega_{q_k,i}\in$ [200 kN/m, 400 kN/m], all drawn from uniform distributions for each member i to model high design complexity. The higher UDLs $\omega_{q_k,i}$ increase the likelihood of deep beams occurring, which increases the chance of critical shear load arrangements, allowing the performance of both algorithms to be stress-tested. Each of the 1024 continuous beam systems were designed against the naive set of load arrangement J_{naive} of size $p_{naive} = 2^m = 1024$, with the most critical load arrangement of each member within each continuous beam system identified. This resulted in $10 \times 1024 = 10,240$ validation data-points. It was subsequently checked if the actual critical load arrangement was represented within the significantly smaller $J_{flex} \cup J_{shear}$ sets.

3.3. Design dataset generation

After validating the critical load arrangement procedure, design datasets were generated under the various design constraints established in Section 3.1. One key consideration is the size of the continuous beam systems in terms of m to model. The number of members m

needs to be at least double the maximum influence size $k_{\rm max}$. This is because the highest influence zone measurable for the middle span of a continuous beam is by design half the system length m. Therefore, size m needs to be chosen such that $\max(\mathbf{k}_{\rm max}) < m/2$, where $\mathbf{k}_{\rm max}$ is the list of all influence values $k_{\rm max}$ of the continuous beam system. A sufficiently large value for m needs to be assumed in case $k_{\rm max}$ is a large value; m=15 was used for this purpose.

Individual design datasets consisting of 32 UDL and 32 span values sampled from a random uniform distribution for a m=15 beam system were created based on the design constraints identified in Section 3.1. Sets 2, 3, and 4, each contained $32\times 32=1024$ continuous beam systems, and since each system contained m=15 members, this resulted in a total of $1024\times 15=15,360$ influence zone values. For Set 1, the difference within the systems only varied in terms of the identical span L and UDLs $\omega_{q_k,i}$ of the members, which were also sampled in 0.5 m and 5 kN/m increments respectively. Given that this results in 23 span and 13 UDL increments for Set 1, Set 1 contained $23\times 13\times 15=4485$ influence zone values.

For the generation of the continuous beam design datasets, a coupled analysis and design approach was taken, optimising for minimum structural depth using third-party software (Rhino3D©, Grasshopper© and Karamba3D© [36]). Design sensitivity analysis was avoided by an implicit ordering of the UKB section list based on structural capacity. The influence zone values were subsequently extracted using Eqs. (2) and (3) based on the procedure visualised in Fig. 4.

4. Results

4.1. Validation of flexural and shear load arrangement algorithms

The validation results for the critical load arrangement identification procedure are illustrated in Fig. 10, which plots the critical load arrangement index for each design beam example. Every load arrangement index corresponds to a unique load arrangement out of the naive set $\mathbf{J}_{\text{naive}}$ of size $p_{\text{naive}} = 2^m = 1024$. The set $\mathbf{J}_{\text{naive}}$ was ordered so that the load arrangements for set \mathbf{J}_{flex} are first, followed by those of set $\mathbf{J}_{\text{shear}}$, and subsequently all others. The design examples themselves were sorted twice: first in ascending number of shear beam occurrences, and subsequently in ascending load arrangement indices. This results in the gradual increase of the J_{crit} indices as seen in Fig. 10.

Fig. 10 sheds insight on a number of important points. The first is that the critical load arrangement $J_{\rm crit}$ for every single beam example from the 10,240 validation dataset occurred within the ${\bf J}_{\rm flex}$ or ${\bf J}_{\rm shear}$ sets. This is strong evidence that the critical load arrangement identification procedure based on polarity sequences zones and polarity zones, as well as Algorithms 1 and 2, are capable of identifying the critical load arrangement of homo- and heterogeneous continuous beam systems. Furthermore, the set size predictions $p_{flex}=2m$ and $p_{shear}=2(m-1)(2^n-1)$ are also confirmed. For the m=10 member system designed here, $p_{flex}=20$, and depending on the number of shear beam occurrences of each system, which varied from $n=\{0,1,2,3,4\}$, the number of shear load arrangements varied from $p_{shear}=\{0,18,54,126,270\}$. This corresponded to $p_{total}=\{20,38,74,146,290\}$ respectively, as indicated by the y-axis of Fig. 10(b).

Fig. 10(a) also emphasises how much smaller sets $J_{\rm flex}$ and $J_{\rm shear}$ are in comparison to $J_{\rm naive}$. This greatly reduces the number of load arrangements that need to be analysed for the influence zone evaluation procedure, whilst also reducing the computational cost of designing the continuous beam system for system lengths of m>10. A summary of these results is shown in Table 2, and further insights are discussed in Section 5.

Table 2 Load arrangements set summary for m dimensional beam systems containing n shear beams with associated algorithm complexities.

Set	Set size	Algorithm complexity
Critical load arrangements per internal beam	6	O(1)
Critical load arrangements per end-span beam	4	O(1)
$J_{ m flex}$ — Critical flexural arrangements per beam system	2 <i>m</i>	O(m)
$\mathbf{J}_{\text{shear}}$ — Critical shear arrangements per beam system	$2(m-1)(2^n-1)$	$O(m^2 2^n)$
J _{naive} — Naive load arrangements	2 ^m	$O(2^m)$

4.2. Influence zone results

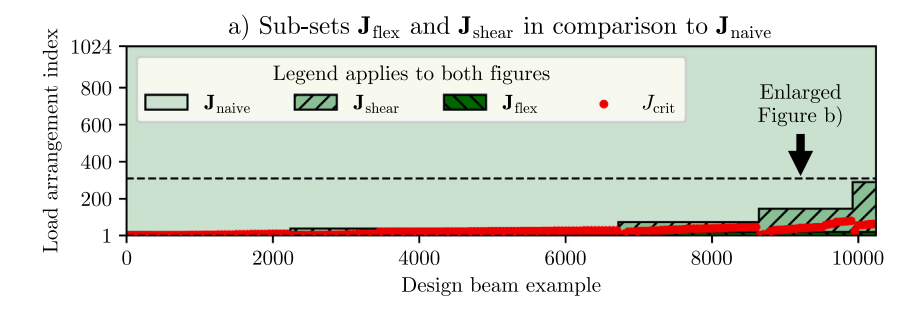
Using the validated critical load arrangement evaluation procedure presented in Section 3.2, various continuous beam systems were generated based on the design constraints highlighted in Sections 3.1 and 3.3. Subsequently, using Eqs. (2) and (3) and the influence zone evaluation procedure visualised in Section 2.4, the influence zone values $k_{\rm max}$ for every member from each system could be evaluated. The influence zone values for one random example from each of the designed continuous beam systems within each dataset (Set 1: Zero Variation, Set 2: Low Variation, Set 3: Medium Variation and Set 4: High Variation, see Table 1) for a maximum error threshold $\epsilon_{\rm max}=0.005$ are shown in Fig. 11.

Within the examples presented in Fig. 11, the influence zone $k_{\rm max}$ can vary for individual members within the same system. For example, in Fig. 11(c), the first member from the left end of the system with a span of $L=9.5\,\rm m$ and a variable (live) UDL value of $\omega_{q_k}=45\,\rm kN/m$ has an influence zone value of $k_{\rm max}=1.$ Within the same system, the fourth member from the right end of the system with a span of $L=3.5\,\rm m$ and $\omega_{q_k}=20\,\rm kN/m$ had an influence zone value of $k_{\rm max}=5.$ Another general observation is that the variability of the influence zone values appears to correlate positively with design complexity (the variability of the spans and UDLs of the system); this can be see comparing the $k_{\rm max}$ values in Set 1 as shown in Fig. 11(a) with those of Set 4 as shown in Fig. 11(d).

The influence zone values of members within continuous beam systems that have already been designed (such as those shown in Fig. 11) shed some insight for structural engineers on whether a design change in terms of a UDL is relevant for a given member (based on whether it falls within that member's influence zone). However, by analysing the distribution of influence zone values of many different homo- and heterogeneous continuous beam systems, it is possible to make that assessment a priori before designing the system itself. Assuming once again a max error threshold $\epsilon_{\rm max} = 0.005$, the aggregated influence zone results for each design set from Table 1 are shown in Fig. 12. For these design datasets, the most common influence zone value (the mode) was $k_{\text{max}} = 3$, and the majority of influence zone values were at $k_{\rm max} \leq$ 3, meaning applied loading information of a given beam along with that of the three adjacent spans on either side captured the correct utilisation ratio of the design beam with an error of less than a $\pm 0.5\%$ in the majority of cases.

However, the various sets reveal differences in the maximum and distribution of the influence zone. The maximum influence zone value for Set 1 was $k_{\rm max}=4$, whereas it was $k_{\rm max}=5$ for Set 2, 3 and 4. Furthermore, as the set number increases, which corresponds with an increase in variation of the design information in terms of spans and UDLs, the influence zone value distribution appears to flatten and widen. For example, it was the high-variation Set 4 which actually contained the most influence zone values $k_{\rm max}=0$ for 1.5% of the design examples. The minimum utilisation curve (red curve with point markers in Fig. 12) captured by each influence zone value suggests that, in general, increasing design variation leads to greater maximum influence zone values.

The average, maximum and 95th percentile influence zone values were also calculated for various error thresholds as shown in Table 3.



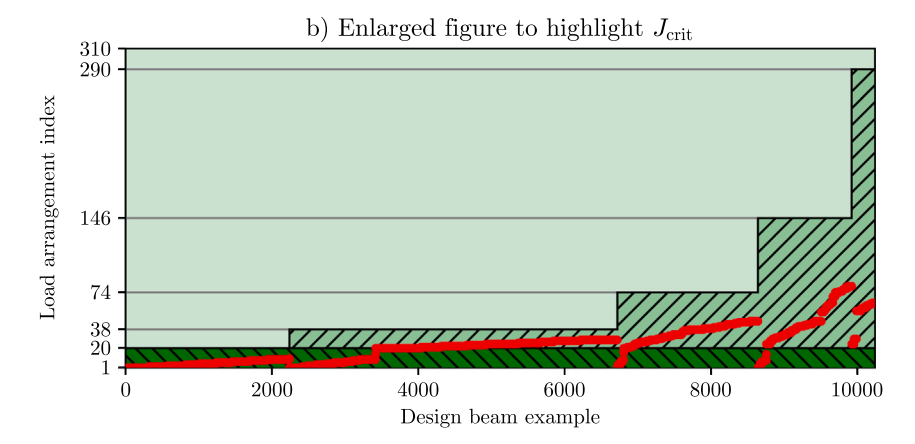


Fig. 10. Load arrangement index for each design beam example ordered in increasing number of shear beam occurrences and critical load arrangement indices. This confirms visually that the critical load arrangement J_{crit} for each design beam example from the generated dataset falls within either J_{flex} or J_{shear} and are significantly smaller than J_{naive} . Figure (b) is an enlarged view of Figure (a).

Table 3 Influence zone results for various maximum error thresholds ϵ_{\max} for each design dataset, evaluating average, maximum and 95th percentile influence zone values k_{\max} . Note that increasing set numbers corresponds with increasing design variation, a proxy for design complexity, see Table 1 for details.

Error $\epsilon_{\rm max}$ [%]	Average k _{max}			Maximum $k_{\rm max}$			95th percentile $k_{\rm max}$					
	Set 1	Set 2	Set 3	Set 4	Set 1	Set 2	Set 3	Set 4	Set 1	Set 2	Set 3	Set 4
0.1	4.60	4.46	3.84	3.37	5	5	6	7	5	5	5	5
0.5	2.89	2.86	2.69	2.38	4	5	5	5	4	4	4	4
1	2.76	2.75	2.35	2.06	3	3	5	5	3	3	3	3
5	1.52	1.39	1.29	1.17	2	3	3	4	2	3	3	3
10	0.98	0.98	0.89	0.83	2	2	3	4	1	1	2	2
20	0.76	0.84	0.73	0.67	1	1	2	3	1	1	1	1
50	0.00	0.30	0.41	0.43	0	1	1	2	0	1	1	1

Note that the maximum influence zone value of $k_{\rm max}=5$ for Set 4 confirms that the m=15 member-size assumption was sufficient for the purpose of this study. Together Fig. 12 and Table 3 provide evidence for the following conclusions:

- A decrease in the acceptable error threshold correlates with an increase in both the influence zone range.
- An increase in design variation correlates with an increase in the maximum influence zone range.
- An increase in design variation, however, correlates with a decrease in average influence zone range in most instances where the acceptable error threshold is relatively tight ($\epsilon_{\rm max} \leq 10\%$). At higher error thresholds the trend is less discernible.

It should be noted that an error threshold of less than 0.5% is relatively small in comparison to uncertainties that exist in structural design. These uncertainties include, for example, material yield strength and imposed UDL values (consider that variable UDL values ω_{q_k} are increased 50% with a load combination factor of 1.5 within the Eurocodes [29]). Furthermore, the design constraints of design set 4 represent the top end of design variation which may occur in typical continuous beam systems. It is therefore reasonable to suggest that for continuous beam systems with design constraints specified in

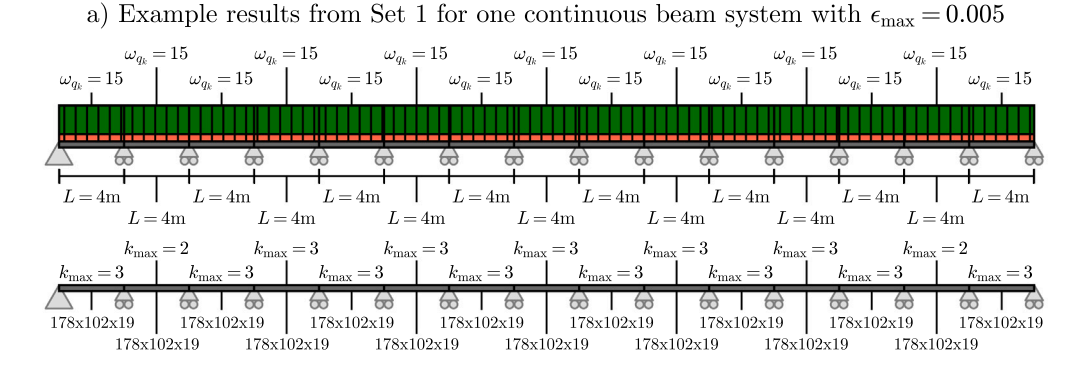
Section 3.1, the influence zone values are on average $k_{\rm max} \leq 3$, with the 95th percentile value being $k_{\rm max} = 4$ and only in the most extreme case $k_{\rm max} = 5$ at an error threshold of less than 0.5%.

5. Discussion

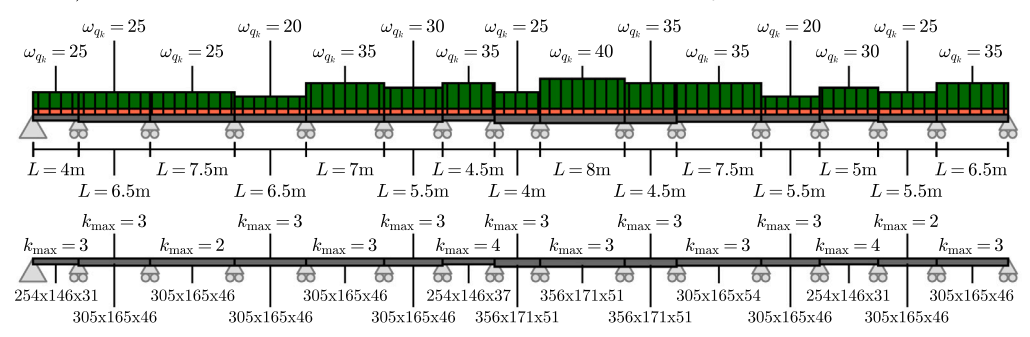
The results along with the proposed evaluation procedures to find the critical load arrangements and influence values for UDL loaded continuous beam systems have led to a number of important findings. These include gaining novel insight on how much surrounding loading information is relevant for a member's design, identifying novel shear load arrangements with the help of polarity zones and polarity sequences, and introducing load arrangement algorithms to explicitly identify critical load arrangements of continuous beam systems of any arbitrary system size. Each of these findings are discussed in detail and contextualised with relevant existing literature.

5.1. Influence zone insights

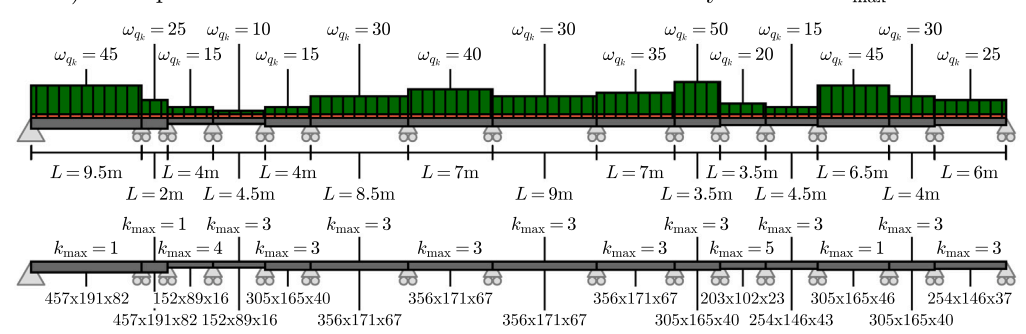
The influence zone results confirm that the impact of loading drops off sharply the further away one moves from the influence line location. This behaviour can be identified across all influence line diagrams







c) Example results from Set 3 for one continuous beam system with $\epsilon_{\rm max} = 0.005$



d) Example results from Set 4 for one continuous beam system with $\epsilon_{\rm max} = 0.005$

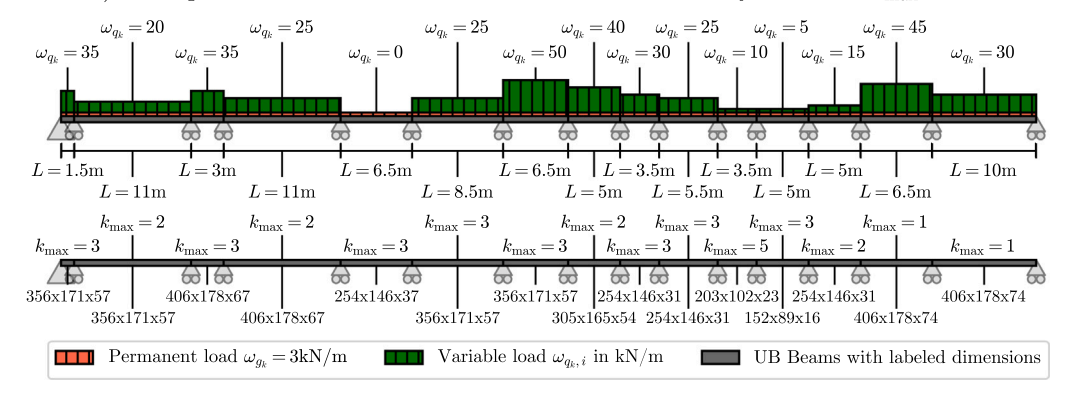


Fig. 11. One example of the influence zone results within continuous beams systems from each design dataset specified in Table 1.

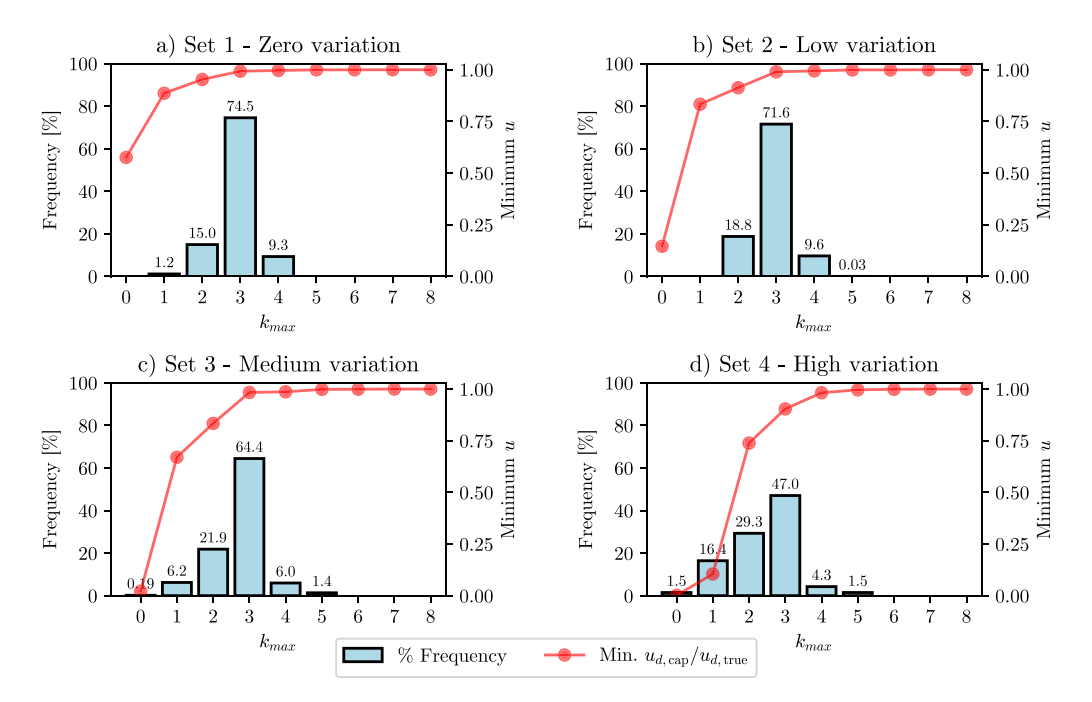


Fig. 12. Influence zone results for various design constraints with a max error threshold $\epsilon_{\max} = 0.005$ indicating the percentage frequency distributions of the influence zone values k_{\max} and minimum utilisation factors captured for each k_{\max} value for a given design beam d.

found within this paper, such as Figs. 5 and 9. This investigation has formulated this concept as the *influence zone*, shown how it applied to continuous beam systems, and rigorously studied the influence zone distributions under various design assumptions and error thresholds. The data related to the dataset generation and influence zone evaluations can be found at an open-source data repository [37].

5.2. Demarcating influence zones from influence lines

Although there is a proximal relationship between the concept of influence zones and influence lines, mostly evidenced by Eq. (3) where integrated influence lines play an important role for the evaluation of influence zones, these two concepts differentiate themselves in important ways. This distinction also applies to the two-dimensional application of influence lines known as influence surfaces [38–41].

Whilst influence lines/surfaces are exact analytical tools that define the mechanical response of a known structural system about a particular point, influence zones are a heuristic design tool that offer insight on what information is relevant to the design of the structural system to begin with based on certain analytical assumptions. The value of influence lines/surfaces arise during analysis on a system-by-system basis, whereas the value of influence zones arise during design after having studied them in their statistical aggregate.

This distinction could be considered further evidence supporting the demarcation between design and analysis in structural engineering. Previous literature has highlighted the difference between *knowledge-that* explains fundamental facts about systems (such as influence lines) versus *knowledge-how* something can be designed or solved (such as influence zones) [42,43]. Recent literature has suggested that the processes of analysis and design solve related, albeit oppositely posed problems known as forward and inverse problems respectively [44]. Influence lines can be seen as a tool that solves the former, whereas influence zones solve the latter.

As a matter of fact, the influence zone concept was developed whilst developing a design model for continuous beam systems from an inverse problem perspective, and allows the *a priori* knowledge of what loading information is relevant for design of a particular continuous beam. It is possible that the influence zone concept could serve as an important heuristic tool in the design of continuous structural

systems, supporting the view that the application of heuristics is a cornerstone for engineering design [45]. Further novel ideas might be uncovered when approaching engineering design from an inverse problem perspective.

5.3. Flexural load arrangements

An important contribution of this investigation was presenting the flexural load arrangements clearly through the use of *polarity sequences*. Notably the *polarity zones* highlight which load arrangement is critical for specific segments of a beam, which could be useful in the design of tapered (non-prismatic) continuous beam systems [46,47].

The influence zone study allows the contextualisation of simplified load arrangement provisions. For example, whilst Annex AB.2 from EN 1993-1-1 [27] covers alternating flexural load arrangements in full, it specifies that for the adjacent flexural load arrangement type, only the two adjacently loaded spans of variable load ω_{q_k} need to be factored. In essence, the variable load information on all other spans aside from the beam under consideration and the two directly adjacent spans are ignored, which is the technical equivalent of assuming an influence zone to $k_{\rm max}=1$.

With help of Table 3, it is possible to infer that an influence zone value $k_{\rm max}=1$ is likely to introduce an error between 5–10% in terms of the true utilisation for design scenarios with no UDL or span variation (the average $k_{\rm max}$ value for $\epsilon_{\rm max}=5\%$ and $\epsilon_{\rm max}=10\%$ is 1.52 and 0.98 for Set 1 respectively). The simplified Eurocode provisions are therefore, on average, a reasonable simplification to capture the impact of variable load arrangements. However, the maximum influence zone value of Set 1 with $k_{\rm max}=1$ corresponds to an error of $\epsilon_{\rm max}=20\%$, and when considering non-heterogeneous continuous beam systems (reflected by Set 2, 3 and 4), this error can increase up to $\epsilon_{\rm max}=50\%$ and more. This is further evidence, as already pointed out in literature, that the load arrangement provisions from building codes can be non-conservative and hence lead to unsafe designs [34].

The simplified provisions within the Eurocodes, which also exist within EN 1992-1-1 5.1.3 [48] and other codes [49], need to be understood in context of the $1.5Q_k$ load factors and the dead load contribution G_k , which invariably will lessen the underestimation made by

the provisions. Nonetheless, the validity of the design code recommendations for flexural load arrangements could be investigated further, especially for highly irregular beam and floor arrangements [50].

5.4. Shear load arrangements

Unlike flexural load arrangements, which have been identified in literature and building codes, the shear load arrangements were a surprising find. To the authors' knowledge, this is the first time that deep beams have been identified to cause new critical load arrangements in literature. Although shear load arrangements sometimes resulted in identical utilisation ratios to that of flexural ones, initial analyses pointed to an average increase in utilisation ratio of 4%–5%, while larger deviations were occasionally observed. Fig. 10 also highlights that these shear load arrangements were relatively prevalent within the design scenarios considered.

Confirmation and validation of these shear load arrangements by future research is encouraged. Of particular interest is why Eq. (5) defines the exact point when these critical load arrangements arise, and whether this equation is valid for all material and cross-section types. One notable difference in the mechanical assumption in this investigation of load arrangements as to that of previous studies was the use of Timoshenko–Ehrenfest rather than Euler–Bernoulli beam theory. For example, the two seminal works on establishing the bounds of critical load arrangements using fuzzy set based finite-element methods used Bernoulli–Euler beam theory [33,34]. A re-investigation with deep beams as defined by Eq. (4) and Timoshenko–Ehrenfest beam theory should reveal more critical bounds of load arrangements than previously identified with interval-finite-element methods. The extent to which these shear load arrangements require special provisions within building codes will require further exploration.

5.5. Critical load arrangement algorithms

The critical load arrangement algorithms provided in Appendices A and B, along with a study of their computational complexity, were key for the evaluation of the influence zone. Limiting the design space to a fraction of the naive J_{naive} load arrangement set without making heuristic simplifications was crucial in both the dataset generation and influence zone evaluation steps. The algorithms have been made available at an open-source data repository [37].

It is likely that there is further room for improvement for Algorithm 2 to evaluate the shear load arrangements for a known list of susceptible shear beams. The current formulation still leads to either pre-existing flexural load arrangements, or creates duplicate shear load arrangements. On average, 74.7% of the outputs obtained from Algorithm Appendix B were unique, with a best-case efficiency of 88.8% and a worst-case efficiency of 12.7%. This suggests that an algorithm with a lesser computational complexity than $O(m^2 \, 2^n)$ might be achievable through further investigation.

5.6. Further influence zone investigations

This investigation will hopefully serve as a starting point for future studies related to the influence zone, including formulations that take more information into account aside from UDL values only. There were several limitations within this study, notably not accounting for serviceability checks and limiting the design space to positively loaded UDLs. The effects of torsion and lateral loading could also be considered. Further studies could be conducted for different material and design information assumptions, while studies could also be expanded to 2D continuous frames and shells, with fixed and semi-rigid connections. The influence zone concept and associated results could be a helpful piece of information when designing any structural system in practical engineering by informing structural engineers on what design information is actually relevant to properly size structural members.

Furthermore, the framing of this novel influence zone concept within structural engineering may encourage awareness in practising engineers on what the size of the influence zone of their particular structural system is, which may have applications in other research areas such as structural health monitoring [51], complex thermomechanical actions on structures [52] and in the development of generalised design models [44].

6. Conclusions

A novel concept termed the *influence zone* was proposed in relation to continuous beam systems. The investigation developed a local and global formulation, of which the latter one was explored numerically with design constraints applicable to steel framed buildings. The key challenge was the explicit definition of critical load arrangements to allow the computational feasible generation of design datasets and evaluation of their respective influence zones. The investigation led to three important outcomes:

- The development of polarity sequences and polarity zones which led to the demarcation between previously known flexural load arrangements and the newly discovered shear load arrangements, with an explicit span limit equation for when these novel load arrangements occur.
- Two algorithms capable of finding these two types of load arrangements, and providing evidence that they encompass all critical permutations in comparison to the naive, brute-force approach.
- The generation of design datasets from which the influence zone values for various degrees of design complexities and error thresholds could be rigorously studied. For error thresholds deemed acceptable in structural design, which in this work was considered to be $\epsilon_{\rm max} \leq 0.5\%$, the influence zone for continuous beams within steel framed building under ultimate state considerations is on average less than 3, going to a maximum influence zone value of 5. This influence zone value is likely to be valid for most design situations whose spans and load values fall within the range of the design constraints considered in Section 3.1.

The influence zone is a heuristic design tool that differentiates itself from influence lines (and influence surfaces) and demonstrates the value of the inverse problem perspective through which it was evaluated by. This study opens the scope for future research, notably in the evaluation of influence zones for various materials and structural systems, validating and explicating the existence of shear load arrangements, and encouraging research on improving the existing algorithm that identifies them.

CRediT authorship contribution statement

Adrien Gallet: Conceptualization, Data curation, Formal analysis, Investigation, Methodology, Project administration, Resources, Software, Validation, Visualization, Writing – original draft, Writing – review & editing. Andrew Liew: Supervision, Writing – review & editing. Iman Hajirasouliha: Supervision, Writing – review & editing. Danny Smyl: Supervision, Validation, Writing – review & editing.

Declaration of competing interest

The authors declare that they have no known competing financial interests or personal relationships that could have appeared to influence the work reported in this paper.

Data availability

Data related to the design datasets and the influence zone results, along with the load arrangement algorithms, are available at an open-source data repository [37].

Funding

The author(s) disclosed receipt of the following financial support for the research, authorship, and/or publication of this article. The authors gratefully acknowledge the support of the Engineering Physical Sciences Research Council's (EPSRC) Doctoral Training Partnership Studentship and the Ramboll Foundation. For the purpose of open access and funding stipulations, the authors have applied a Creative Commons Attribution (CC-BY) licence to any Accepted Manuscript (AM) version arising.

Appendix A. Algorithm 1 - Flexural load arrangements

```
1 # Create the alternating load arrangements — altLoadArr
   if m % 2 == 0: altLoadArr = [[1,0]*(m//2)]
   else: altLoadArr = [[1,0]*(m//2) + [1]]
   # Create the adjacent load arrangements — adjLoadArr
   adjLoadArr = []
   if m > 1:
       for i in range(m-1):
           # Create the start loadArr
10
           if i % 2 == 0: startLoadArr = [1,0]*(i//2)
           else: startLoadArr = [0,1]*(i//2) + [0]
12
           # Create the end loadArr
           if (m-i) \% 2 == 0: endLoadArr = [0,1]*((m-i-2)//2)
14
15
           else: endLoadArr = [0,1]*((m-i-2)//2) + [0]
16
17
           # Append loadArr together with adjacent loaded spans
18
           adjLoadArr.append(startLoadArr + [1,1] + endLoadArr)\\
19
   # Create positive J_flex load arrangements
20
   J_flex_pos = altLoadArr + adjLoadArr
21
   # Evaluate polar opposites — negative J_flex
23
   J flex neg = []
   for loadArr in J_flex_pos:
25
       J_flex_neg.append([1 if act == 0 else 0])
                          for act in loadArr])
   # Evaluate J_flex
   J_flex = J_flex_pos + J_flex_neg
```

Algorithm 1: Flexural load arrangement algorithm in Python with both alternating and adjacent arrangements for a continuous beam system with m members that creates set \mathbf{J}_{flex} with $\mathbf{O}(m)$ time complexity.

Appendix B. Algorithm 2 - Shear load arrangements

```
# Function to identify shear load arrangements
   def shearLoadArr(loadArr: list, shearBeams: list, start: int):
       # Iterate in both directions
       for direction in [-1, 1]:
            # Establish while loop variables
           finishing = False; finished = False
           updating = False; i = start
           # Iterate through the beam system
           while finished == False:
10
                i = i + direction # Move to the next beam
               # Case 1: End of beam system is reached
13
               if i < 0 or i >= len(loadArr):
15
                    finished = True
16
               # Case 2: No shear beam has been encountered yet
                elif updating == False and finishing == False:
18
19
                    # Check if current beam is a shear beam
20
                    if i in shearBeams:
21
                        updating = True; updateAct = loadArr[i]
23
               # Case 3: A shear beam has been encountered
               elif updating == True and finishing == False:
24
                     Update activation factor of current beam
                    loadArr[i] = updateAct
```

```
# Check if current beam is a shear beam
2.7
28
                    if i not in shearBeams:
29
                        updating = False; finishing = True
30
31
               # Case 4: Alternate remaining activation factors
32
                elif finishing == True:
33
                   loadArr[i] = (loadArr[i-direction] + 1) % 2
34
35
                    # If another shear beam is encountered
36
                    if i in shearBeams:
37
                        updateAct = loadArr[i]
38
                        updating = True; finishing = False
39
       return loadArr
```

Algorithm 2: Shear load arrangement algorithm in Python to generate arrangements belonging to set J_{shear} based on a given flexural load arrangements loadArr, the indices of susceptible *shearBeams*, starting at beam index *start*, for a system size with m members, with n shear beams. One single pass has a time complexity of O(m), yet generating the entire set J_{shear} is $O(m^2 2^n)$.

References

- [1] Betti E. Teoria della elasticita. Il Nuovo Cimento 1872;7–8(1):5–21. http://dx.doi.org/10.1007/BF02824590.
- [2] Blake LS, editor. Civil engineer's reference book. Elsevier; 1989, http://dx.doi. org/10.1016/C2013-0-00875-4.
- [3] Karnovsky IA, Lebed O. Advanced methods of structural analysis. Boston, MA: Springer US; 2010, http://dx.doi.org/10.1007/978-1-4419-1047-9.
- [4] Hibbeler RC. Structural analysis. 9th ed.. Upper Saddle River, N.J. Pearson Prentice Hall: 2015.
- [5] Hosur V, Bhavikatti S. Influence lines for bending moments in beams on elastic foundations. Comput Struct 1996;58(6):1225–31. http://dx.doi.org/10. 1016/0045-7949(95)00219-7.
- [6] Fiorillo G, Ghosn M. Application of influence lines for the ultimate capacity of beams under moving loads. Eng Struct 2015;103:125–33. http://dx.doi.org/10. 1016/j.engstruct.2015.09.003.
- Buckley E. Basic influence line equations for continuous beams and rigid frames. J Struct Eng 1997;123(10):1416–20. http://dx.doi.org/10.1061/(ASCE) 0733-9445(1997)123:10(1416).
- [8] Zheng X, Yang D-H, Yi T-H, Li H-N. Development of bridge influence line identification methods based on direct measurement data: A comprehensive review and comparison. Eng Struct 2019;198:109539. http://dx.doi.org/10.1016/j.engstruct. 2019.109539.
- [9] Zhu X, Law S. Structural health monitoring based on vehicle-bridge interaction: Accomplishments and challenges. Adv Struct Eng 2015;18(12):1999–2015. http://dx.doi.org/10.1260/1369-4332.18.12.1999.
- [10] Chen Z-W, Cai Q-L, Zhu S. Damage quantification of beam structures using deflection influence lines. Struct Control Health Monit 2018;25(11):e2242. http: //dx.doi.org/10.1002/stc.2242.
- [11] Zheng X, Yang D-H, Yi T-H, Li H-N. Bridge influence line identification from structural dynamic responses induced by a high-speed vehicle. Struct Control Health Monit 2020;27(7). http://dx.doi.org/10.1002/stc.2544.
- [12] Kuklik P. Zone of influence. In: Bobrowsky P, Marker B, editors. Encyclopedia of engineering geology. Cham: Springer International Publishing; 2018, p. 1–2. http://dx.doi.org/10.1007/978-3-319-12127-7-309-1.
- [13] Yang J. Influence zone for end bearing of piles in sand. J Geotech Geoenviron Eng 2006;132(9):1229–37. http://dx.doi.org/10.1061/(ASCE)1090-0241(2006) 132:9(1229).
- [14] Ekanayake S, Liyanapathirana D, Leo C. Influence zone around a closed-ended pile during vibratory driving. Soil Dyn Earthq Eng 2013;53:26–36. http://dx.doi. org/10.1016/j.soildyn.2013.06.005.
- [15] Kuklík P, Kopáčková M. Efficient analytical model for calculation of the influence zone inside the subsoil below foundations slabs. Acta Polytech 2004;44(5–6). http://dx.doi.org/10.14311/632.
- [16] Cao C, Xu Z, Chai J, Qin Y, Cao J. Determination method for influence zone of pumped storage underground cavern and drainage system. J Hydrol 2021;595:126018. http://dx.doi.org/10.1016/j.jhydrol.2021.126018.
- [17] Jakovovic D, Werner AD, de Louw PG, Post VE, Morgan LK. Saltwater upconing zone of influence. Adv Water Resour 2016;94:75–86. http://dx.doi.org/10.1016/ j.advwatres.2016.05.003.
- [18] Goel A, Kumar P. Zone of influence for particle number concentrations at signalised traffic intersections. Atmos Environ 2015;123:25–38. http://dx.doi. org/10.1016/j.atmosenv.2015.10.054.
- [19] Alvin M, Adhinugraha KM, Alamri S, Mir U. Influence zone expansion for reverse k nearest neighbours query. Multimedia Tools Appl 2021. http://dx.doi.org/10. 1007/s11042-021-11275-3.

- [20] Cheema MA, Zhang W, Lin X, Zhang Y. Efficiently processing snapshot and continuous reverse k nearest neighbors queries. VLDB J 2012;21(5):703–28. http://dx.doi.org/10.1007/s00778-012-0265-y.
- [21] Yoshizawa K, Kennett BLN. Determination of the influence zone for surface wave paths. Geophys J Int 2002;149(2):440–53. http://dx.doi.org/10.1046/j.1365-246X.2002.01659.x.
- [22] Casper BB, Schenk HJ, Jackson RB. Defining a plant's belowground zone of influence. Ecology 2003;84(9):2313–21. http://dx.doi.org/10.1890/02-0287.
- [23] Schlueter A, Thesseling F. Building information model based energy/exergy performance assessment in early design stages. Autom Constr 2009;18(2):153–63. http://dx.doi.org/10.1016/j.autcon.2008.07.003.
- [24] Sinclair D, Tait A, Carmichael L. RIBA plan of work overview. 2020.
- [25] Mason J, Manning M. Structural design: the engineer's role. London: Institution of Structural Engineers; 2011.
- [26] Saka MP, Geem ZW. Mathematical and metaheuristic applications in design optimization of steel frame structures: An extensive review. Math Probl Eng 2013;2013;1–33. http://dx.doi.org/10.1155/2013/271031.
- [27] CEN. BS EN 1993-1-1:2005+A1:2014 Eurocode 3. Design of steel structures. General rules and rules for buildings. BSI British Standards; 2015, http://dx.doi.org/10.3403/03270565.
- [28] CEN. BS EN 10365:2017 Hot rolled steel channels, I and H sections. Dimensions and masses. BSI British Standards: 2017. http://dx.doi.org/10.3403/30318327.
- [29] CEN. BS EN 1990:2002+A1:2005 Eurocode. Basis of structural design. BSI British Standards; 2010, http://dx.doi.org/10.3403/02612036.
- [30] Shiryayev AN. Interpolation and extrapolation of stationary random sequences. In: Shiryayev AN, editor. Selected works of A. N. Kolmogorov. Springer Netherlands; 1992, p. 272–80. http://dx.doi.org/10.1007/978-94-011-2260-3_28
- [31] Zadeh L. Fuzzy sets. Inf Control 1965;8(3):338–53. http://dx.doi.org/10.1016/ S0019-9958(65)90241-X
- [32] Zadeh L. Fuzzy sets as a basis for a theory of possibility. Fuzzy Sets and Systems 1999;100:9–34. http://dx.doi.org/10.1016/S0165-0114(99)80004-9.
- [33] Köylüoğlu HU, Çakmak AŞ, Nielsen SRK. Interval algebra to deal with pattern loading and structural uncertainties. J Eng Mech 1995;121(11):1149–57. http: //dx.doi.org/10.1061/(ASCE)0733-9399(1995)121:11(1149).
- [34] Mullen RL, Muhanna RL. Bounds of structural response for all possible loading combinations. J Struct Eng 1999;125(1):98–106. http://dx.doi.org/10.1061/ (ASCE)0733-9445(1999)125:1(98).
- [35] Labuschagne A, Van Rensburg N, Van Der Merwe A. Comparison of linear beam theories. Math Comput Modelling 2009;49(1–2):20–30. http://dx.doi.org/ 10.1016/j.mcm.2008.06.006.
- [36] Preisinger C. Linking structure and parametric geometry. Archit Des 2013;83(2):110-3. http://dx.doi.org/10.1002/ad.1564.
- [37] Gallet A, Smyl D. IZ Kmax: influence zone results and design datasets. 2024, http://dx.doi.org/10.15131/shef.data.24433918.
- [38] Deng L, Wu H, He W, Ling T, Liu G. Genuine influence line and influence surface identification from measured bridge response considering vehicular wheel loads. J Bridge Eng 2023;28(2):04022145. http://dx.doi.org/10.1061/JBENF2.BEENG-5604.

- [39] Zheng X, Yang D-H, Yi T-H, Li H-N. Bridge influence surface identification method considering the spatial effect of vehicle load. Struct Control Health Monit 2021;28(8). http://dx.doi.org/10.1002/stc.2769.
- [40] Orakdogen E, Girgin K. Direct determination of influence lines and surfaces by F.E.M.. Struct Eng Mech 2005;20(3):279–92. http://dx.doi.org/10.12989/SEM. 2005.20.3.279.
- [41] Memari A, West H. Computation of bridge design forces from influence surfaces. Comput Struct 1991;38(5-6):547-56. http://dx.doi.org/10.1016/0045-7949(91) 90006-8
- [42] Bulleit WM. What makes an engineering education an engineering education? In: Structures congress 2012. Chicago, Illinois, United States: American Society of Civil Engineers; 2012, p. 1143–51. http://dx.doi.org/10.1061/9780784412367.
- [43] Bulleit W, Schmidt J, Alvi I, Nelson E, Rodriguez-Nikl T. Philosophy of engineering: what it is and why it matters. J Prof Issues Eng Educ Pract 2015;141(3):02514003. http://dx.doi.org/10.1061/(ASCE)EI.1943-5541. 0000205.
- [44] Gallet A, Rigby S, Tallman TN, Kong X, Hajirasouliha I, Liew A, Liu D, Chen L, Hauptmann A, Smyl D. Structural engineering from an inverse problems perspective. Proc R Soc Lond Ser A Math Phys Eng Sci 2022;478(2257):20210526. http://dx.doi.org/10.1098/rspa.2021.0526.
- [45] Koen BV. Discussion of the method: conducting the engineer's approach to problem solving. New York: Oxford University Press; 2003.
- [46] Kaveh A, Kabir MZ, Bohlool M. Optimal design of multi-span pitched roof frames with tapered members. Period Polytech Civ Eng 2018. http://dx.doi.org/10. 3311/PPci.13107.
- [47] Veenendaal D, Coenders J, Vambersky J, West M. Design and optimization of fabric-formed beams and trusses: Evolutionary algorithms and form-finding. Struct Concr 2011;12(4):241–54. http://dx.doi.org/10.1002/suco.201100020.
- [48] CEN. BS EN 1992-1-1 Eurocode 2: Design of concrete structures part 1-1: general rules and rules for buildings. British Standards Institution; 2015, http://dx.doi.org/10.3403/03178016U.
- [49] Technical Committee. Code of practice for structural use of concrete 2013. Hong Kong: Buildings Department; 2020.
- [50] Ho DYB. Pattern load analyses for irregular floor systems. Proc Inst Civ Eng -Struct Build 2015;168(6):433–40. http://dx.doi.org/10.1680/stbu.13.00116.
- [51] Yang D-H, Yi T-H, Li H-N, Zhang Y-F. Correlation-based estimation method for cable-stayed bridge girder deflection variability under thermal action. J Perform Constr Facil 2018;32(5):04018070. http://dx.doi.org/10.1061/(ASCE)CF.1943-5509.0001212.
- [52] Yang D-H, Yi T-H, Li H-N, Zhang Y-F. Monitoring and analysis of thermal effect on tower displacement in cable-stayed bridge. Measurement 2018;115:249–57. http://dx.doi.org/10.1016/j.measurement.2017.10.036.